# Robust topological design of the actuator-coupled structures with hybrid uncertainties

Z. C. He[a,c], H. X. Jiang[a], Y. Wu[a], Eric Li[b*], B Zhou[d], Q Tang[d,e]

[a]*State Key Laboratory of Advanced Design and Manufacturing for Vehicle Body, Hunan University, Changsha, 410082 P. R. China*

[b]*School of Science, Engineering & Design, Teesside University, Middlesbrough, UK*

[c]*Guangxi Key Laboratory of Automobile Components and Vehicle technology, Guangxi University of Science and Technology, Liuzhou, 545006, P. R. China*

[d]*Department of Mechanical Engineering, Hunan Institute of Engineering, Xiangtan 411101, PR China*

[e]*Hunan Province Key Laboratory of Vehicle Power and Transmission System, Xiangtan 411101, China*

## Abstract

Based on the bi-directional evolutionary structural optimization (BESO) method, a robust topology optimization (RTO) algorithm is developed for the actuator-coupled structures with hybrid uncertainties. The hybrid interval random variables (HIRV) model is adopted to simulate the uncertainty of the mechanical and piezoelectric parameters. The worst case of the compliance is set as the robust objective function. A hybrid uncertainty perturbation analysis method (HUPAM) is proposed to estimate the expectation and standard variance of the robust objective function. The density-based interpolation scheme is employed to establish the design variables, and the sensitivity of the robust objective function with respect to the design variables is derived. The robust topologies of the host structure and the optimal placement of the coupled actuators are obtained by the proposed RTO approach. Several numerical examples are presented to show the effectiveness of the proposed method and the Monte Carlo method (MCM) is used to validate the accuracy of the HUPAM.

*Keywords***:** Robust topology optimization; Actuator-coupled structures; Hybrid uncertainties; Perturbation analysis method.

*Corresponding author: Tel./fax: +86 73188822051.

*Email address:* ericsg2012@gmail.com (Eric Li)

## 1. Introduction

Piezoelectric materials are capable of converting electrical energy into mechanical one, and vice versa [1]. This property allows opportunities for sensing [2], actuating [3] and energy harvesting [4]. In general the active components made of piezoelectric materials are integrated in structures to form smart structures. Due to the presence of the active components like actuators and sensors, the traditional deterministic structures acquire new functionality or achieve lightweight without losing its mechanical performance [5,6]. Consider the demand of structural control in practical engineering, piezoelectric actuators can be a good choice to achieve active control with its advantages in high energy density and fast response [7]. In general, piezoelectric actuators are bonded on the surface of the host structure or embedded in the host structure. Therefore, the actuator-coupled structures (AS) are introduced for structural control in this study. For the AS, the elastic material constitutes the host structure, while the piezoelectric actuators form the active control part which is employed to weaken the effects of external excitations.

The efficient structural control design of AS needs an optimal structural topology and the careful selection of actuator positions. Topology optimization is considered a powerful tool for structural design at the conceptual design stage. The basic goal of topology optimization is to find an efficient use of the amount of material through an iterative numerical process in a fixed domain [8]. Since Bendsøe and Kikuchi [9] first introduced the concept of topology optimization, many advanced methods [10-13] have been proposed in the past decades. These methods have successfully applied to many physical situations to date, such as the design of compliant mechanisms [14], metamaterials [15] and piezoelectric systems [16]. As an extension, the interpolation schemes [11] based on multi-material problem, which increases design freedom for better solution in practical engineering, were proposed. The method is widely adopted in topology optimization of integrated structures and many scholars have gained some achievements in piezoelectric actuator-coupled structures. Martin and Emílio [17] proposed a new optimization method to design the piezoelectric plate and shell actuators by using solid isotropic material with penalization (SIMP) model. In this way, piezoelectric actuators can achieve a maximum output displacement in a given direction at a given point of the structure. Carbonar et al. [18] presented a formulation of simultaneous optimization problem for non-piezoelectric and piezoelectric structure. Aim at the maximal output displacements or output forces, the optimization design of the piezoceramic position and the piezoceramic rotation angles is considered in the paper. Zheng et al. [19] considered the layout of elastic and piezoelectric materials without predefined the shape or position of piezoceramic. Kang et al. [20] incorporated the actuation voltage into the design by establishing an interpolation between the applied voltage and the design variable. They optimized the material layout and

the voltage distribution for maximizing the specified nodal displacement. Wang et al. [21] formulated an integrated topology optimization problem for the compliant structures with embedded movable actuators. The method is employed to optimize positions and angle of the piezoelectric actuators in the optimized host structure. However, most studies in the field are carried out based on the deterministic assumptions.

With the continuous increase in complexity of structural control systems, the influence of the uncertainty on the structural components becomes more remarkable. On the one hand, the uncertainties due to material properties, geometric dimensions and manufacturing tolerances are widespread in practical engineering [22]. Besides, the integrated use of actuators is affected by multiphysical systems, which should be fully considered in coupling structures [23]. Therefore, it is essential to deal with the uncertain information for AS. Generally, uncertainty is divided into two categories: probabilistic-based uncertainty [24,25] and non-probabilistic uncertainty [26-30]. For probabilistic-based uncertainty, probabilistic method is considered as an effective strategy to deal with traditional structural uncertainty analysis when sufficient experimental samples are provided. However, it is often difficult to establish accurate probability distributions of the uncertain parameters due to testing difficulties and high cost in many actual engineering. In addition, the experimental samples with poor quality can also affect the credibility of design results [31]. Thus, the imprecise probability uncertainty with limited information is most likely obtained. In such situations, hybrid interval random model is introduced to describe the uncertain parameters which are assumed to follow the probabilistic distribution with interval value [32]. Since lots of structural optimization problems are influenced by both aleatory and epistemic uncertainties, the hybrid uncertainty method is developed to deal with probabilistic and non-probabilistic uncertainties, simultaneously. Among the existing hybrid uncertainty method [33-35], the hybrid interval random uncertainty [36,37] is effective to describe the uncertainty with imprecise probability distribution.

To deal with uncertainty in topology optimization problems, the methods of reliability-based topology optimization (RBTO) and robust topology optimization (RTO) are widely adopted. For RBTO problems [38-41], the optimization considers uncertainty in the constraints through a reliability index. For instance, Jalalpour and Tootkaboni [42] solved the RBTO problem under material uncertainty. Wang et al. [43] developed a non-probabilistic RBTO method for continuum structures with unknown but bounded uncertainties. RTO [44-46] aims to minimize the variance or both the mean and variance of the objective function. For instance, Chen et al. [47] proposed a RTO methodology for continuum structures with interval random uncertainties by using the hybrid stochastic interval perturbation method. He et al. [32] introduced the interval random parameters into topology optimization for dynamic properties involving dynamic-compliance

and eigenvalue. Zheng et al. [48] developed the dynamic topology optimization method for concurrent design problems with the random-interval hybrid uncertainties. Since most structures are involved the hybrid uncertainties, the proposed method in this paper has incorporated the interval random variables into topology optimization problem of the AS. An efficient HUPAM was also proposed to calculate the worst case of the objective function which was expressed as a linear combination of the mean and standard variance.

The remainder of this paper is organized as follows. Section 2 briefly introduces the finite element model of the piezoelectricity and describes the formulations of topology optimization problems. In Section 3, the hybrid interval random variables are presented to simulate the imprecise probability distribution and the hybrid uncertainty perturbation analysis method is given to calculate the maximal expectation and standard variance of the considered interval random variables. In order to obtain the optimal structural topologies and actuators placement, Section 4 gives a robust topological design algorithm of the AS to minimize the objective function. In Section 5, the numerical implementation of the proposed algorithm is shown. Several numerical examples are given in Section 6 to illustrate the effectiveness of the proposed method. Finally, conclusions are presented.

## 2. Theoretical background

In this section, finite element analysis of piezoelectricity and topology optimization formulation of the AS are given. The numerical algorithm is employed to obtain the optimal topologies and the optimal placement of the piezoelectric actuators. Fig. 1 shows the AS that is filled with piezoelectric phase, non-piezoelectric phase and void phase.

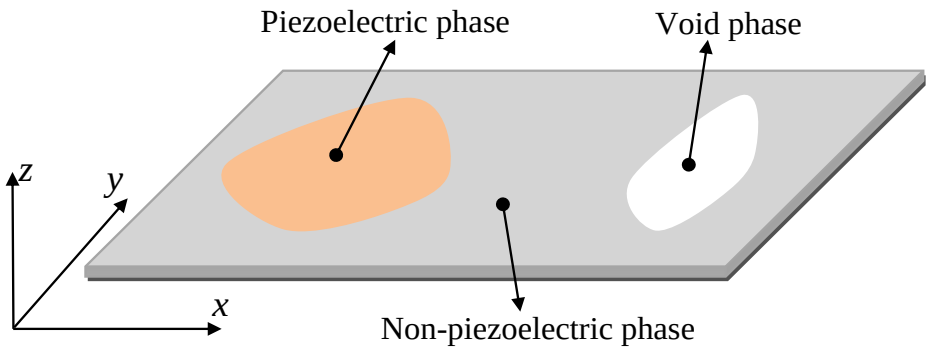


**Fig.1** The actuator-coupled structure

### *2.1 Piezoelectric finite element formulation*

When a piezoelectric material is deformed, there is an electric polarization in the material, resulting in an electric potential difference. On the contrary, the potential difference in the material causes the deformation of piezoelectric material. Assume that the piezoelectric material has a linear response under the

changes in electric displacement, electric field, mechanical stress and strain. The electromechanical coupling effect can be expressed by the following constitutive equation

$$\begin{aligned}\mathbf{T} &= \mathbf{C}^E\mathbf{S} - \mathbf{e}^T\mathbf{E} \\ \mathbf{D} &= \mathbf{e}\mathbf{S} + \boldsymbol{\kappa}^S\mathbf{E}\end{aligned} \tag{1}$$

where $\mathbf{T}$ and $\mathbf{S}$ denote the stress and strain vectors respectively. $\mathbf{D}$ and $\mathbf{E}$ stand for the electric displacement and electric field vectors respectively. The material coefficient matrices, $\mathbf{C}^E$, $\mathbf{e}$, and $\boldsymbol{\kappa}^S$ indicate the stress-strain relation under a constant electric field, the piezoelectric coupling, and the permittivity under constant strain, respectively. The superscript, *T*, refers to the transpose of matrices.

Further, Eq. (1) can be rewritten as

$$\begin{bmatrix}\sigma_x\\ \sigma_y\\ \sigma_z\\ \tau_{yz}\\ \tau_{zx}\\ \tau_{xy}\end{bmatrix} = \begin{bmatrix}C_{11} & C_{12} & C_{13} & 0 & 0 & 0\\ C_{12} & C_{22} & C_{23} & 0 & 0 & 0\\ C_{13} & C_{23} & C_{33} & 0 & 0 & 0\\ 0 & 0 & 0 & C_{44} & 0 & 0\\ 0 & 0 & 0 & 0 & C_{55} & 0\\ 0 & 0 & 0 & 0 & 0 & C_{66}\end{bmatrix}\begin{bmatrix}\varepsilon_x\\ \varepsilon_y\\ \varepsilon_z\\ \gamma_{yz}\\ \gamma_{zx}\\ \gamma_{xy}\end{bmatrix} - \begin{bmatrix}0 & 0 & e_{31}\\ 0 & 0 & e_{32}\\ 0 & 0 & e_{33}\\ 0 & e_{24} & 0\\ e_{15} & 0 & 0\\ 0 & 0 & 0\end{bmatrix}\begin{bmatrix}E_x\\ E_y\\ E_z\end{bmatrix} \tag{2}$$

$$\begin{bmatrix}D_x\\ D_y\\ D_z\end{bmatrix} = \begin{bmatrix}0 & 0 & 0 & 0 & e_{15} & 0\\ 0 & 0 & 0 & e_{24} & 0 & 0\\ e_{31} & e_{32} & e_{33} & 0 & 0 & 0\end{bmatrix}\begin{bmatrix}\varepsilon_x\\ \varepsilon_y\\ \varepsilon_z\\ \gamma_{yz}\\ \gamma_{zx}\\ \gamma_{xy}\end{bmatrix} + \begin{bmatrix}\kappa_{11} & 0 & 0\\ 0 & \kappa_{22} & 0\\ 0 & 0 & \kappa_{33}\end{bmatrix}\begin{bmatrix}E_x\\ E_y\\ E_z\end{bmatrix} \tag{3}$$

Assume that the electric potential is applied linearly in the *z*-direction of the piezoelectric elements, the electric field vector $\mathbf{E}$ of the piezoelectric element is

$$\mathbf{E}=\begin{bmatrix}E_x & E_y & E_z\end{bmatrix}^T = \begin{bmatrix}0 & 0 & \dfrac{V_e}{h}\end{bmatrix}^T \tag{4}$$

where $h$ is the thickness of the actuator layer and $V_e$ is the voltage of the piezoelectric element.

Based on Hamilton's principle, the piezoelectric finite element matrix equations for global system can be expressed as

$$\begin{bmatrix}\mathbf{K}_{uu} & \mathbf{K}_{u\phi}\\ \mathbf{K}_{u\phi}^T & \mathbf{K}_{\phi\phi}\end{bmatrix}\begin{Bmatrix}\mathbf{u}\\ \boldsymbol{\varphi}\end{Bmatrix} = \begin{Bmatrix}\mathbf{F}_u\\ \mathbf{Q}_\phi\end{Bmatrix} \tag{5}$$

where

$$\mathbf{K}_{uu} = \sum_e \int_{\Omega_e} \mathbf{B}_u^T\mathbf{C}^E\mathbf{B}_u d\Omega_e = \sum_e \mathbf{k}_{uu}^e \tag{6a}$$

$$\mathbf{K}_{u\phi} = \sum_e \int_{\Omega_e} \mathbf{B}_u^T \mathbf{e} \mathbf{B}_\phi d\Omega_e = \sum_e \mathbf{k}_{u\phi}^e \tag{6b}$$

$$\mathbf{K}_{\phi\phi} = -\sum_e \int_{\Omega_e} \mathbf{B}_\phi^T \boldsymbol{\kappa}^S \mathbf{B}_\phi d\Omega_e = \sum_e \mathbf{k}_{\phi\phi}^e \tag{6c}$$

In Eq. (5) and Eq. (6), the terms $\mathbf{k}_{u\phi}^e$, $\mathbf{k}_{uu}^e$ and $\mathbf{k}_{\phi\phi}^e$ represent the piezoelectric coupling matrix, structural stiffness matrix and dielectric conductivity matrix of the element, respectively. $\mathbf{B}_u$ is the matrix relating the strain with displacement and $\mathbf{B}_\phi$ is the matrix connecting the electrical field with the electrical potential. $\mathbf{u}$ and $\boldsymbol{\varphi}$ denote the global displacement and electric potential global vectors, respectively.

In Eq. (5), the mechanical loads vector and electrical loads vector are defined as

$$\mathbf{F}_u = \sum_e \left( \int_{\Omega_e} \mathbf{N}_u^T \mathbf{f}_b^e d\Omega_e + \int_{A_e} \mathbf{N}_u^T \mathbf{f}_s^e dA_e + \mathbf{N}_u^T \mathbf{f}_c^e \right) \tag{7}$$

$$\mathbf{Q}_\phi = -\sum_e \int_{A_e} \mathbf{N}_\phi^T \mathbf{q}_s^e dA_e - \mathbf{N}_\phi^T \mathbf{q}_c^e \tag{8}$$

where $\mathbf{N}_u$ and $\mathbf{N}_\phi$ denote the matrices of the displacement interpolation function and the electrical potential interpolation function, respectively. The symbols $\mathbf{f}_b^e$, $\mathbf{f}_s^e$, and $\mathbf{f}_c^e$ are the applied body force vector, the surface traction vector and the concentrated forces vector of the element, respectively. The $\mathbf{q}_s^e$ and $\mathbf{q}_c^e$ represent the surface electric loads vector and the concentrated electric loads vector of the element, respectively.

In order to simplify the process of analyzing the equilibrium equation of the piezoelectric system, Eq. (5) can be rewritten as

$$\mathbf{K}\mathbf{U} = \mathbf{F} \tag{9}$$

where

$$\mathbf{K} = \begin{bmatrix} \mathbf{K}_{uu} & \mathbf{K}_{u\phi} \\ \mathbf{K}_{u\phi}^T & \mathbf{K}_{\phi\phi} \end{bmatrix} \quad \mathbf{U} = \begin{Bmatrix} \mathbf{u} \\ \boldsymbol{\varphi} \end{Bmatrix} \quad \mathbf{F} = \begin{Bmatrix} \mathbf{F}_u \\ \mathbf{Q}_\phi \end{Bmatrix} \tag{10}$$

*2.2 Optimization problem statement and formulation*

*2.2.1 Interpolation scheme*

Two design variables, one of them represents the elastic material distribution of the host structure and another represents the location of the actuators, are considered. To obtain the gradient information of the design variables, multi-material interpolation theory proposed by SIMP method is adopted which can be expressed as

$$\mathbf{C}^{E}\left(x_a, x_p\right) = x_a^{p_{cu}}\left(x_p^{p_{c\phi}}\mathbf{C}_p^{E} + \left(1 - x_p^{p_{c\phi}}\right)\mathbf{C}_a^{E}\right) \tag{11}$$

$$\mathbf{e}\left(x_a, x_p\right) = x_a^{p_{cu}} x_p^{p_{ee}}\mathbf{e}_p \tag{12}$$

$$\boldsymbol{\kappa}^{S}\left(x_a, x_p\right) = x_a^{p_{cu}} x_p^{p_{\kappa\kappa}}\boldsymbol{\kappa}_p^{S} \tag{13}$$

where $\mathbf{C}_a^E$ and $\mathbf{C}_p^E$ are the characteristic matrices of the non-piezoelectric material and the piezoelectric material, respectively. $\mathbf{e}_p$, and $\boldsymbol{\kappa}_p^S$ are the characteristic matrices of the piezoelectric coupling and the permittivity, respectively. $P_{cu}$, $P_{c\phi}$, $P_{ee}$, and $P_{\kappa\kappa}$ represent the exponents of the penalization and their values are both set to be 3. $x_a$ and $x_p$ denote the element design variable of the non-piezoelectric phase and the piezoelectric phase, respectively.

*2.2.2 Optimization problem statement*

The aim of topology optimization is to find the optimal distribution in a fixed domain that satisfies prescribed constrains and minimizes a predefined objective. Thus, the optimization problem of classical minimum compliance can be formulated as

$$\text{Minimize: } C_d\left(u, \phi, x_a, x_p\right) = \mathbf{u}^T\mathbf{K}_{uu}\mathbf{u} + \mathbf{u}^T\mathbf{K}_{u\phi}\boldsymbol{\varphi} + \boldsymbol{\varphi}^T\mathbf{K}_{u\phi}^T\mathbf{u} + \boldsymbol{\varphi}^T\mathbf{K}_{\phi\phi}\boldsymbol{\varphi} \tag{14}$$

$$\begin{aligned} &\text{Subject to: } \mathbf{K}_{uu}\mathbf{u} + \mathbf{K}_{u\phi}\boldsymbol{\varphi} = \mathbf{F}_u \\ &\qquad \mathbf{K}_{u\phi}^T\mathbf{u} + \mathbf{K}_{\phi\phi}\boldsymbol{\varphi} = \mathbf{Q}_\phi \\ &\qquad \sum_{e=1}^{N_e} x_{a_e} V_e \le \alpha V_0 \\ &\qquad \sum_{e=1}^{N_e} x_{p_e} V_e \le \beta V_0 \\ &\text{where: } x_{a_e} = x_{\min} \text{ or } 1,\ x_{p_e} = x_{\min} \text{ or } 1 \quad (e = 1, \ldots, N_e) \end{aligned} \tag{15}$$

where $C_d$ is the objective function value. The parameters $\alpha$ and $\beta$ denote the volume fraction of the solid of the non-piezoelectric material and piezoelectric material, respectively. $V_0$ represents the volume of design domain. $x_{a_e} = 1$ and $x_{a_e} = x_{\min}$ are the solid elements and void elements of the non-piezoelectric material, respectively. $x_{p_e} = 1$ and $x_{p_e} = x_{\min}$ are the solid elements and void elements of the piezoelectric material, respectively. To avoid the singularity of the matrices, $x_e = x_{\min} = 0.001$ is used in this paper. $N_e$ is the total number of finite elements.

*2.2.3 Sensitivity analysis*

The sensitivities of the objective function with respect to the element design variables can be calculated efficiently through the adjoint method [49]. By introducing a constant multiple $\boldsymbol{\lambda}$ of the equality constraint for calculating the sensitivity, the objective function is modified to

$$C_d = \mathbf{F}^T\mathbf{U} + \boldsymbol{\lambda}^T\left(\mathbf{F} - \mathbf{K}\mathbf{U}\right) \tag{16}$$

The sensitivity of the objective function $C_d$ with respect to the design variables $x_{i_e}$ can be expressed as

$$\frac{\partial C_d}{\partial x_{i_e}} = \left(\mathbf{F} - \mathbf{K}\boldsymbol{\lambda}\right)^T \frac{\partial \mathbf{U}}{\partial x_{i_e}} - \boldsymbol{\lambda}^T \frac{\partial \mathbf{K}}{\partial x_{i_e}}\mathbf{U} \tag{17}$$

The arbitrary constant $\boldsymbol{\lambda}$ is chosen to satisfy $\mathbf{K}\cdot\boldsymbol{\lambda} = \mathbf{F}$. Thus, the Eq. (17) can be rewritten as

$$\frac{\partial C_d}{\partial x_{i_e}} = -\mathbf{U}^T \frac{\partial \mathbf{K}}{\partial x_{i_e}}\mathbf{U} \tag{18}$$

Substituting Eq. (6) and Eq. (11-13) into Eq. (18), the sensitivities of the objective function $C_d$ with respect to the design variables $x_a$ and $x_p$ can be expressed as

$$\begin{aligned}\frac{\partial C_d}{\partial x_{a_e}} = &-\sum_{e=1}^{N_e} p_{cu}\left(x_{a_e}\right)^{p_{cu}-1}\left[\left(x_{p_e}\right)^{p_{c\phi}}\left(\mathbf{u}^e\right)^T\mathbf{k}_{dp}^e\mathbf{u}^e + \left(1-\left(x_{p_e}\right)^{p_{c\phi}}\right)\left(\mathbf{u}^e\right)^T\mathbf{k}_{da}^e\mathbf{u}^e\right]\\ &-\sum_{e=1}^{N_e} p_{cu}\left(x_{a_e}\right)^{p_{cu}-1}\left(x_{p_e}\right)^{p_{ee}}\left(\mathbf{u}^e\right)^T\mathbf{k}_{u\phi}^e\boldsymbol{\varphi}^e - \sum_{e=1}^{N_e} p_{cu}\left(x_{a_e}\right)^{p_{cu}-1}\left(x_{p_e}\right)^{p_{ee}}\left(\boldsymbol{\varphi}^e\right)^T\left(\mathbf{k}_{u\phi}^e\right)^T\mathbf{u}^e\\ &-\sum_{e=1}^{N_e} p_{cu}\left(x_{a_e}\right)^{p_{cu}-1}\left(x_{p_e}\right)^{p_{\kappa\kappa}}\left(\boldsymbol{\varphi}^e\right)^T\mathbf{k}_{\phi\phi}^e\boldsymbol{\varphi}^e\end{aligned} \tag{19}$$

$$\begin{aligned}\frac{\partial C_d}{\partial x_{p_e}} = &-\sum_{e=1}^{N_e} p_{c\phi}\left(x_{a_e}\right)^{p_{cu}}\left(x_{p_e}\right)^{p_{c\phi}-1}\left(\left(\mathbf{u}^e\right)^T\mathbf{k}_{dp}^e\mathbf{u}^e - \left(\mathbf{u}^e\right)^T\mathbf{k}_{da}^e\mathbf{u}^e\right)\\ &-\sum_{e=1}^{N_e} p_{ee}\left(x_{a_e}\right)^{p_{cu}}\left(x_{p_e}\right)^{p_{ee}-1}\left(\mathbf{u}^e\right)^T\mathbf{k}_{u\phi}^e\boldsymbol{\varphi}^e - \sum_{e=1}^{N_e} p_{ee}\left(x_{a_e}\right)^{p_{cu}}\left(x_{p_e}\right)^{p_{ee}-1}\left(\boldsymbol{\varphi}^e\right)^T\left(\mathbf{k}_{u\phi}^e\right)^T\mathbf{u}^e\\ &-\sum_{e=1}^{N_e} p_{\kappa\kappa}\left(x_{a_e}\right)^{p_{cu}}\left(x_{p_e}\right)^{p_{\kappa\kappa}-1}\left(\boldsymbol{\varphi}^e\right)^T\mathbf{k}_{\phi\phi}^e\boldsymbol{\varphi}^e\end{aligned} \tag{20}$$

where $\mathbf{k}_{da}^e$ and $\mathbf{k}_{dp}^e$ represent the stiffness of the element of the non-piezoelectric material and piezoelectric material that can be expressed as

$$\mathbf{k}_{da}^e = \int_{\Omega_e}\mathbf{B}_u^T\mathbf{C}_a^E\mathbf{B}_u d\Omega_e \tag{21}$$

$$\mathbf{k}_{dp}^e = \int_{\Omega_e}\mathbf{B}_u^T\mathbf{C}_p^E\mathbf{B}_u d\Omega_e \tag{22}$$

## 3. Mathematical formulation of HIRV and HUPAM

*3.1 Hybrid interval random variable (HIRV)*

It is assumed that $\mathbf{X}(\mathbf{Y})$ denotes the interval random vector of all interval random variables. $X_r(r=1,2,\cdots,\xi)$ is the *r*-th random parameter of the interval probabilistic distribution variables $Y_e(e=1,2,\cdots,\gamma)$. The expression of each interval variable $Y_e$ is formulated as $\left[Y_e^L, Y_e^U\right]$. $Y_e^L$ and $Y_e^U$ represent the lower and upper bounds value of $Y_e$ respectively. $Y_e^M = \dfrac{Y_e^U + Y_e^L}{2}$ and $Y_e^R = \dfrac{Y_e^U - Y_e^L}{2}$ are the interval mean value and the maximum interval radius of $Y_e$ respectively.

Based on the above definition, the expectation $\mu\left(\mathbf{X}(\mathbf{Y})\right)$ and variance $\sigma^2\left(\mathbf{X}(\mathbf{Y})\right)$ is written as

$$\mu\left(\mathbf{X}(\mathbf{Y})\right) = \mu\left(X_1(\mathbf{Y}), X_2(\mathbf{Y}), ....., X_\xi(\mathbf{Y})\right) \tag{23a}$$

$$\sigma^2\left(\mathbf{X}(\mathbf{Y})\right) = \sigma^2\left(X_1(\mathbf{Y}), X_2(\mathbf{Y}), ....., X_\xi(\mathbf{Y})\right) \tag{23b}$$

*3.2 Hybrid uncertainty perturbation analysis method (HUPAM)*

To obtain the worst situation with uncertain parameters, HUPAM is proposed which is divided into two steps to get the effective hybrid interval random variables. In the first step, assume the interval variables $\mathbf{Y}$ of the interval random variables $\mathbf{X}(\mathbf{Y})$ are the constant value, so the interval random function $\Re\left(\mathbf{X}(\mathbf{Y})\right)$ at the expectation $\mu\left(\mathbf{X}(\mathbf{Y})\right)$ can be formulated by the first-order Taylor expansion

$$\Re\left(\mathbf{X}(\mathbf{Y})\right) = \Re\left(\mu\left(\mathbf{X}(\mathbf{Y})\right)\right) + \sum_{r=1}^{\xi} \frac{\partial \Re\left(\mu\left(\mathbf{X}(\mathbf{Y})\right)\right)}{\partial X_r}\left(X_r - \mu\left(X_r(\mathbf{Y})\right)\right) + \Re_1\left(\mathbf{X}(\mathbf{Y})\right) \tag{24}$$

As a result, $\Re\left(\mathbf{X}(\mathbf{Y})\right)$ is divided into three parts. The last part $\Re_1\left(\mathbf{X}(\mathbf{Y})\right)$ is a relatively small error caused by the Taylor expansion which can be ignored in this work, and the first two parts are called the expectation $E(\Re)$ and standard variance $SD(\Re)$ respectively, which is expressed as

$$E(\Re) = \Re\left(\mu\left(\mathbf{X}(\mathbf{Y})\right)\right) \tag{25a}$$

$$SD(\Re) = \sum_{r=1}^{\xi} \frac{\partial \Re\left(\mu\left(\mathbf{X}(\mathbf{Y})\right)\right)}{\partial X_r} \sigma\left(X_r(\mathbf{Y})\right) \tag{25b}$$

In the second step, considering that the interval variable $\mathbf{Y}$ is not a constant, the expectation and the standard variance are also the interval vectors with respect to the interval variables. By the hybrid uncertainty

perturbation analysis method, the first-order Taylor expansion is adopted again for $E(\Re)$ and $SD(\Re)$ at the interval mean value $Y_e^M$, which can be expressed as

$$\begin{aligned}\mathrm{E}(\Re) &= \Re\left(\mu\left(\mathbf{X}\left(\mathbf{Y}^M\right)\right)\right)+\sum_{r=1}^{\xi}\sum_{e=1}^{\gamma}\left[\begin{array}{l} sign\left(\dfrac{\partial\Re\left(\mu\left(\mathbf{X}\left(\mathbf{Y}^M\right)\right)\right)}{\partial\mu\left(X_r\left(\mathbf{Y}\right)\right)}\dfrac{\partial\mu\left(X_r\left(\mathbf{Y}^M\right)\right)}{\partial Y_e^M}Y_e^R\right) \\ \dfrac{\partial\Re\left(\mu\left(\mathbf{X}\left(\mathbf{Y}^M\right)\right)\right)}{\partial\mu\left(X_r\left(\mathbf{Y}\right)\right)}\dfrac{\partial\mu\left(X_r\left(\mathbf{Y}^M\right)\right)}{\partial Y_e^M}Y_e^R\end{array}\right]+\Re_2\left(\mathbf{Y}\right) \\ &=\Re_0+\sum_{r=1}^{\xi}\sum_{e=1}^{\gamma}\Re_{1,r}\frac{\partial\mu\left(X_r\left(\mathbf{Y}^M\right)\right)}{\partial Y_e^M}Y_e^R S_1+\Re_2\left(\mathbf{Y}\right)\end{aligned} \tag{26a}$$

$$\begin{aligned}\mathrm{SD}(\Re) &= \sum_{r=1}^{\xi}\left[\begin{array}{l}\dfrac{\partial\Re\left(\mu\left(\mathbf{X}\left(\mathbf{Y}^M\right)\right)\right)}{\partial X_r}\sigma\left(X_r\left(\mathbf{Y}^M\right)\right)+ \\ \sum_{e=1}^{\gamma}\left(\begin{array}{l} sign\left(\dfrac{\partial^2\Re\left(\mu\left(\mathbf{X}\left(\mathbf{Y}^M\right)\right)\right)}{\partial X_r\partial Y_e^M}\sigma\left(X_r\left(\mathbf{Y}^M\right)\right)Y_e^R\right)\dfrac{\partial^2\Re\left(\mu\left(\mathbf{X}\left(\mathbf{Y}^M\right)\right)\right)}{\partial X_r\partial Y_e^M}\sigma\left(X_r\left(\mathbf{Y}^M\right)\right)Y_e^R+ \\ sign\left(\dfrac{\partial\Re\left(\mu\left(\mathbf{X}\left(\mathbf{Y}^M\right)\right)\right)}{\partial X_r}\dfrac{\partial\sigma\left(X_r\left(\mathbf{Y}^M\right)\right)}{\partial Y_e^R}Y_e^R\right)\dfrac{\partial\Re\left(\mu\left(\mathbf{X}\left(\mathbf{Y}^M\right)\right)\right)}{\partial X_r}\dfrac{\partial\sigma\left(X_r\left(\mathbf{Y}^M\right)\right)}{\partial Y_e^R}Y_e^R\end{array}\right) \\ +\Re_3\left(\mathbf{Y}\right)\end{array}\right] \\ &=\sum_{r=1}^{\xi}\left(\Re_{2,r}\sigma\left(X_r\left(\mathbf{Y}^M\right)\right)+\sum_{e=1}^{\gamma}\Re_{3,re}\sigma\left(X_r\left(\mathbf{Y}^M\right)\right)Y_e^R S_2+\sum_{e=1}^{\gamma}\Re_{2,r}\frac{\partial\sigma\left(X_r\left(\mathbf{Y}^M\right)\right)}{\partial Y_e^R}Y_e^R S_3+\Re_3\left(\mathbf{Y}\right)\right)\end{aligned} \tag{26b}$$

where $\Re_2(\mathbf{Y})$ and $\Re_3(\mathbf{Y})$ are the error terms and $S_1$, $S_2$ and $S_3$ are the associated symbolic functions. $\Re_0$, $\Re_{1,r}$, $\Re_{2,r}$ and $\Re_{3,re}$ in Eq. (26) are expressed as

$$\Re_0=\Re\left(\mu\left(\mathbf{X}\left(\mathbf{Y}^M\right)\right)\right) \tag{27a}$$

$$\Re_{1,r}=\frac{\partial\Re\left(\mu\left(\mathbf{X}\left(\mathbf{Y}^M\right)\right)\right)}{\partial\mu\left(X_r\left(\mathbf{Y}\right)\right)} \tag{27b}$$

$$\Re_{2,r}=\frac{\partial\Re\left(\mu\left(\mathbf{X}\left(\mathbf{Y}^M\right)\right)\right)}{\partial X_r} \tag{27c}$$

$$\Re_{3,re}=\frac{\partial^2\Re\left(\mu\left(\mathbf{X}\left(\mathbf{Y}^M\right)\right)\right)}{\partial X_r\partial Y_e^M} \tag{27d}$$

## 4. Robust topology optimization formulation

### *4.1 Optimization formulation*

With hybrid interval random variables, the optimization objective function can be rewritten as

$$C\left(\mathbf{X}\left(\mathbf{Y}\right)\right)=\mathbf{U}\left(\mathbf{X}\left(\mathbf{Y}\right)\right)^{T}\mathbf{K}\left(\mathbf{X}\left(\mathbf{Y}\right)\right)\mathbf{U}\left(\mathbf{X}\left(\mathbf{Y}\right)\right) \tag{28}$$

In robust topology optimization, the objective function is represented as a linear combination of the mean and standard variance. In order to minimize both the mean and standard variance of objective, the robust optimization problem is reformulated as

$$\begin{aligned}&\text{Minimize}: C_{max}=E\left(C_d\right)_{max}+\kappa SD\left(C_d\right)_{max} \\ &\text{Subject to}: \mathbf{K}\left(\mathbf{X}\left(\mathbf{Y}\right)\right)\mathbf{U}\left(\mathbf{X}\left(\mathbf{Y}\right)\right)=\mathbf{F}\left(\mathbf{X}\left(\mathbf{Y}\right)\right) \\ &\qquad \sum_{e=1}^{N_e}x_{a_e}V_e\le\alpha V_0 \\ &\qquad \sum_{e=1}^{N_e}x_{p_e}V_e\le\beta V_0 \\ &\text{where}: x_{a_e}=x_{\min}\ or\ 1,\ x_{p_e}=x_{\min}\ or\ 1\quad (e=1,...,N_e)\end{aligned} \tag{29-30}$$

where $\kappa$ denotes the weight of the standard variance. $E\left(\cdot\right)_{max}$ and $SD\left(\cdot\right)_{max}$ are the maximum value of the expectation and standard variance respectively.

Substituting the mean value of interval random vector $\mu\left(\mathbf{X}\left(\mathbf{Y}^{M}\right)\right)$ into Eq. (30), we can get

$$\mathbf{K}\left(\mu\left(\mathbf{X}\left(\mathbf{Y}^{M}\right)\right)\right)\mathbf{U}\left(\mu\left(\mathbf{X}\left(\mathbf{Y}^{M}\right)\right)\right)=\mathbf{F}\left(\mu\left(\mathbf{X}\left(\mathbf{Y}^{M}\right)\right)\right) \tag{31}$$

From the above, the interval random vector $\mathbf{U}$, which corresponds to the structural properties and external load, is a direct response during the optimization procedure. Based on the mathematical formulation in Eq. (31), the displacement field vector $\mathbf{U}_0$ and its derivatives $\mathbf{U}_{1,r}$, $\mathbf{U}_{2,r}$, $\mathbf{U}_{3,re}$ can be derived as

$$\mathbf{U}_0=\mathbf{K}\left(\mu\left(\mathbf{X}\left(\mathbf{Y}^{M}\right)\right)\right)^{-1}\mathbf{F}\left(\mu\left(\mathbf{X}\left(\mathbf{Y}^{M}\right)\right)\right) \tag{32a}$$

$$\mathbf{U}_{1,r}=-\mathbf{K}\left(\mu\left(\mathbf{X}\left(\mathbf{Y}^{M}\right)\right)\right)^{-1}\frac{\partial\mathbf{K}\left(\mu\left(\mathbf{X}\left(\mathbf{Y}^{M}\right)\right)\right)}{\partial\mu\left(X_r\left(\mathbf{Y}\right)\right)}\mathbf{U}_0 \tag{32b}$$

$$\mathbf{U}_{2,r}=-\mathbf{K}\left(\mu\left(\mathbf{X}\left(\mathbf{Y}^{M}\right)\right)\right)^{-1}\frac{\partial\mathbf{K}\left(\mu\left(\mathbf{X}\left(\mathbf{Y}^{M}\right)\right)\right)}{\partial X_r}\mathbf{U}_0 \tag{32c}$$

$$\mathbf{U}_{3,re}=-\mathbf{K}\left(\mu\left(\mathbf{X}\left(\mathbf{Y}^{M}\right)\right)\right)^{-1}\left[2\frac{\partial\mathbf{K}\left(\mu\left(\mathbf{X}\left(\mathbf{Y}^{M}\right)\right)\right)}{\partial X_r}\mathbf{U}_{2,r}+\frac{\partial^2\mathbf{K}\left(\mu\left(\mathbf{X}\left(\mathbf{Y}^{M}\right)\right)\right)}{\partial X_r\partial Y_e}\mathbf{U}_0\right] \tag{32d}$$

Combined the above equations with HUPAM, the maximum values of expectation $E\left(C_d\right)_{max}$ and standard variance $SD\left(C_d\right)_{max}$ are formulated as

$$E\left(C_d\right)_{max}=\mathbf{F}^{T}\mathbf{U}_0+\sum_{r=1}^{\xi}\sum_{e=1}^{\gamma}\mathbf{F}^{T}\mathbf{U}_{1,r}\frac{\partial\mu\left(X_r\left(\mathbf{Y}^{M}\right)\right)}{\partial Y_e^{M}}Y_e^{M}S_1 \tag{33a}$$

$$SD\left(C_d\right)_{max}=\sum_{r=1}^{\xi}\left[\mathbf{F}^T\mathbf{U}_{2,r}\sigma\left(X_r\left(\mathbf{Y}^M\right)\right)+\sum_{e=1}^{\gamma}\left(\begin{array}{l}\mathbf{F}^T\mathbf{U}_{3,re}\sigma\left(X_r\left(\mathbf{Y}^M\right)\right)Y_e^RS_2\\+\mathbf{F}^T\mathbf{U}_{2,r}\dfrac{\partial\sigma\left(X_r\left(\mathbf{Y}^M\right)\right)}{\partial Y_e^R}Y_e^RS_3\end{array}\right)\right] \tag{33b}$$

where $\mathbf{F}$ denotes external excitation.

*4.2 Sensitivity analysis*

The sensitivity of the robust objective function $C_{max}$ with respect to the design variables $x_{i_e}$ can be calculated by the following equation

$$\frac{\partial C_{max}}{\partial x_{i_e}}=\frac{\partial E\left(C_d\right)_{max}}{\partial x_{i_e}}+\kappa\frac{\partial SD\left(C_d\right)_{max}}{\partial x_{i_e}} \tag{34}$$

where $x_{i_e}$ is employed to represent the element design variables. From Eq. (34) $\dfrac{\partial E\left(C_d\right)_{max}}{\partial x_{i_e}}$ and $\dfrac{\partial SD\left(C_d\right)_{max}}{\partial x_{i_e}}$ can be derived as

$$\frac{\partial E\left(C_d\right)_{max}}{\partial x_{i_e}}=\frac{\partial\mathbf{F}^T\mathbf{U}_0}{\partial x_{i_e}}+\sum_{r=1}^{\xi}\sum_{e=1}^{\gamma}\frac{\partial\mathbf{F}^T\mathbf{U}_{1,r}}{\partial x_{i_e}}\frac{\partial\mu\left(X_r\left(\mathbf{Y}^M\right)\right)}{\partial Y_e^M}Y_e^MS_1 \tag{35a}$$

$$\frac{\partial SD\left(C_d\right)_{max}}{\partial x_{i_e}}=\sum_{r=1}^{\xi}\left[\frac{\partial\mathbf{F}^T\mathbf{U}_{2,r}}{\partial x_{i_e}}\sigma\left(X_r\left(\mathbf{Y}^M\right)\right)+\sum_{e=1}^{\gamma}\left(\begin{array}{l}\dfrac{\partial\mathbf{F}^T\mathbf{U}_{3,re}}{\partial x_{i_e}}\sigma\left(X_r\left(\mathbf{Y}^M\right)\right)Y_e^RS_2\\+\dfrac{\partial\mathbf{F}^T\mathbf{U}_{2,r}}{\partial x_{i_e}}\dfrac{\partial\sigma\left(X_r\left(\mathbf{Y}^M\right)\right)}{\partial Y_e^R}Y_e^RS_3\end{array}\right)\right] \tag{35b}$$

where

$$\frac{\partial\mathbf{F}^T\mathbf{U}_0}{\partial x_{i_e}}=\mathbf{U}_0^T\frac{\partial\mathbf{K}\left(\mu\left(\mathbf{X}\left(\mathbf{Y}^M\right)\right)\right)}{\partial x_{i_e}}\mathbf{U}_0 \tag{36a}$$

$$\frac{\partial\mathbf{F}^T\mathbf{U}_{1,r}}{\partial x_{i_e}}=\mathbf{U}_0^T\frac{\partial^2\mathbf{K}\left(\mu\left(\mathbf{X}\left(\mathbf{Y}^M\right)\right)\right)}{\partial x_{i_e}\partial\mu\left(X_r\left(\mathbf{Y}\right)\right)}\mathbf{U}_0+\mathbf{U}_0^T\frac{\partial\mathbf{K}\left(\mu\left(\mathbf{X}\left(\mathbf{Y}^M\right)\right)\right)}{\partial x_{i_e}}\mathbf{U}_{1,r}+\mathbf{U}_{1,r}^T\frac{\partial\mathbf{K}\left(\mu\left(\mathbf{X}\left(\mathbf{Y}^M\right)\right)\right)}{\partial x_{i_e}}\mathbf{U}_0 \tag{36b}$$

$$\frac{\partial\mathbf{F}^T\mathbf{U}_{2,r}}{\partial x_{i_e}}=\frac{\partial\mathbf{F}^T\mathbf{U}_{1,r}}{\partial x_{i_e}}\frac{\partial\mu\left(X_r\left(\mathbf{Y}\right)\right)}{\partial X_r} \tag{36c}$$

$$\frac{\partial\mathbf{F}^T\mathbf{U}_{3,re}}{\partial x_{i_e}}=2\left(\begin{array}{l}\mathbf{U}_0^T\dfrac{\partial^2\mathbf{K}\left(\mu\left(\mathbf{X}\left(\mathbf{Y}^M\right)\right)\right)}{\partial x_{i_e}\partial X_r}\mathbf{U}_{2,r}+\mathbf{U}_{2,r}^T\dfrac{\partial^2\mathbf{K}\left(\mu\left(\mathbf{X}\left(\mathbf{Y}^M\right)\right)\right)}{\partial x_{i_e}\partial X_r}\mathbf{U}_0\\+\mathbf{U}_{2,r}^T\dfrac{\partial\mathbf{K}\left(\mu\left(\mathbf{X}\left(\mathbf{Y}^M\right)\right)\right)}{\partial x_{i_e}}\mathbf{U}_{2,r}+\mathbf{U}_0^T\dfrac{\partial\mathbf{K}\left(\mu\left(\mathbf{X}\left(\mathbf{Y}^M\right)\right)\right)}{\partial x_{i_e}}\mathbf{U}_{3,re}\end{array}\right)+\mathbf{U}_0^T\frac{\partial^3\mathbf{K}\left(\mu\left(\mathbf{X}\left(\mathbf{Y}^M\right)\right)\right)}{\partial x_{i_e}\partial X_r\partial Y_e}\mathbf{U}_0 \tag{36d}$$

## 5. Optimization algorithms

In this paper, the BESO method is applied to obtain the optimal convergent solution. To ensure the existence of the optimal solution, some algorithms such as the numerical filter scheme, the average of the sensitivity value and the convergence criterion are adopted for the topology optimization iterative procedure with hybrid interval random variables. The main steps are outlined in this section.

### *5.1 Numerical implementation*

In order to prevent checkerboard and mesh-dependence [50,51], a filter scheme is applied to update the sensitivity number, which is expressed as

$$\hat{\alpha}_i = \frac{\sum_{e=1}^{N} w(r_{ie})\alpha_e}{\sum_{e=1}^{N} w(r_{ie})} \tag{37}$$

where $r_{ie}$ represents the distance between the center of element $i$ and node $e$. $w(r_{ie})$ is the linear weight factor defined as

$$w(r_{ie}) = \begin{cases} r_{\min} - r_{ie} & \text{for } r_{ie} < r_{\min} \\ 0 & \text{for } r_{ie} \geq r_{\min} \end{cases} \tag{38}$$

where $r_{\min}$ is the predefined filter radius.

Average the sensitivity numbers with their historical information is used to help stabilize the optimization procedure [51], which is given as

$$\hat{\alpha}_i = \frac{\hat{\alpha}_i^k + \hat{\alpha}_i^{k-1}}{2} \tag{39}$$

where $k$ is the number of current iteration.

Once the prescribed volume constraints are satisfied, the optimization procedure continues until the objective function converges. The convergence criterion can be written as

$$error = \frac{\left| \sum_{e=1}^{N} C_{k-e+1} - \sum_{e=1}^{N} C_{k-5-e+1} \right|}{\sum_{e=1}^{N} C_{k-e+1}} \leq \tau \tag{40}$$

where $C_k$ is the objective function value of the *k*-th iteration, and $\tau$ represents the tolerance of change.

### *5.2 Optimization procedure*

The process of the robust topology optimization method of the AS with hybrid interval random variables is outlined as follows:

Step 1: Discretize the design domain into a finite element mesh and define the loads and the boundary conditions.

Step 2: Define the BESO parameters, such as the target volumes fraction $\alpha$ and $\beta$, the evolutionary ratio ER and the filter radius $r_{\min}$.

Step 3: Introduce hybrid interval random variables into the AS.

Step 4: Carry out the finite element analysis and calculate the expectation and standard variance of the objective function.

Step 5: Compute the elemental sensitivity values of the objective function with respect to the elemental design variables $x_a$ and $x_p$.

Step 6: Filter elemental sensitivity number using Eq. (37) and average the sensitivity with their historical information using Eq. (39).

Step 7: Determine the target volume of material for next design. When the current volume of material 1 $V_1^k$ is larger than the given objective volume, reduce the volume of material 1 as

$$V_1^{k+1} = V_1^k \left(1 - ER\right) \tag{41}$$

If the calculated $V_1^{k+1}$ is less than the objective volume, then set $V_1^{k+1}$ to be the $V_1^k$. Similarly, when $V_1^k$ is less than the objective volume, increase the volume of material 1 as

$$V_1^{k+1} = V_1^k \left(1 + ER\right) \tag{42}$$

If the resulting $V_1^{k+1}$ is larger than $V_1^k$, then $V_1^{k+1}$ is set to be equal to $V_1^k$.

Step 8: Update the design variables of all elements on sensitivity analysis.

Step 9: Repeat Steps 4-8 until the volume constraints are satisfied and the objective function is convergent.

## 6. Numerical examples

In this section, numerical examples are presented to verify the proposed method. For all examples, the volume constraints are set to be $\alpha = 0.4$ and $\beta = 0.1$. The property parameters of the AS are assumed to be hybrid interval random variables. In order to demonstrate the influence of uncertainties, the optimized results of deterministic designs and robust designs are given. The robust objective function values of both deterministic designs and robust designs are provided for comparison. Monte Carlo Method (MCM) is also used to validate the accuracy of the proposed method. In all cases, the Young's modulus and Poisson's ratio of piezoelectric material and non-piezoelectric material are set as $E_1 = E_2 = 7.0 \times 10^{10}\ \mathrm{N/m^2}$, $\nu_1 = \nu_2 = 0.3$, and

the piezoelectric constants and relative permittivity are given as $e_{31} = -9.6\ \mathrm{C/m^2}$, $e_{33} = 15.1\ \mathrm{C/m^2}$, $e_{15} = 12.0\ \mathrm{C/m^2}$, $\kappa_{11} = 1700$, $\kappa_{33} = 1750$.

The Young's modulus, Poisson's ratio and piezoelectric constant are assumed to be interval random variables and follow the normal distribution. The intervals of the expectation and standard variance of the uncertain parameters are given as follows:

$$\mu(E_1) = [6.3, 7.7] \times 10^{10}\ \mathrm{N/m^2},\ \sigma(E_1) = [0.63, 0.77] \times 10^{10}\ \mathrm{N/m^2} \tag{43a}$$

$$\mu(\nu_1) = [0.285, 0.315],\ \sigma(\nu_1) = [0.01425, 0.01575] \tag{43b}$$

$$\mu(E_2) = [6.3, 7.7] \times 10^{10}\ \mathrm{N/m^2},\ \sigma(E_2) = [0.63, 0.77] \times 10^{10}\ \mathrm{N/m^2} \tag{43c}$$

$$\mu(\nu_2) = [0.285, 0.315],\ \sigma(\nu_2) = [0.01425, 0.01575] \tag{43d}$$

$$\mu(e_{31}) = [-10.08, -9.12]\ \mathrm{C/m^2},\ \sigma(e_{31}) = [-0.504, -0.456]\ \mathrm{C/m^2} \tag{43e}$$

where $\mu$ and $\sigma$ denote the expectation and standard variance, respectively. During the optimization process, the potential is applied along the *z*-axis and the evolutionary ratio is set to be 0.02. The termination criterion of iteration is that the relative difference of the objective function values is less than 0.001 between two successive iterations. For all the figures of optimized designs, the red color denotes the piezoelectric material, while the blue color indicates the non-piezoelectric material.

*6.1 Example 1*

A cantilever beam is investigated for structural design. The structure with the length $L = 90mm$ and the height $H = 30mm$, is shown in Fig. 2, and the left side is fixed. A concentrated load ($F = 1N$) is applied on the middle point of the right side. The design domain is discretized with $90 \times 30$ quadrilateral elements.

The optimized designs are given in Figs. 3 and 4. Fig. 3 and Fig. 4(a) show the results of the deterministic design and Fig. 4(b-d) are the results of the robust design with different weight coefficient. $C$ denotes the compliance with deterministic parameters and $C_{max}$ represents the optimized objective function values with uncertain parameters. Compare Fig. 3 with Fig. 4(a), the optimized objective function value $C$ of deterministic design of the non-piezoelectric structure is larger than that of the AS. This indicates that the actuators based on piezoelectric effects make a contribution to improve the structural performance. From the final results in Fig .4, the robust designs are much different from the deterministic design. The robust designs have a slight change when the weight coefficients are different.

Monte Carlo method is employed to verify the accuracy of the proposed method in robust topology

optimization. In the simulation of the optimal design under uncertain parameters based on MCM, both the number of samples of interval variables and random parameters are set to be $10^3$, which makes the total number of samples reach to be $10^6$. Table 1 shows the maximal objective function values (including maximal expectation and standard variance) of the optimized designs using HUPAM and MCM. For validation purpose, the relative errors of the maximal expectation and standard variance for each situation are listed. It shows that the objective function values calculated by the proposed method and the MCM are very close. The values of robust optimized results with different weights and the deterministic optimized result are used for comparison. It can be seen that the maximal expectation and standard variance of the robust design is smaller than that of the deterministic design. These illustrate that the uncertainties have a great effect on the structural design and the proposed method is effective for robust topology optimization.

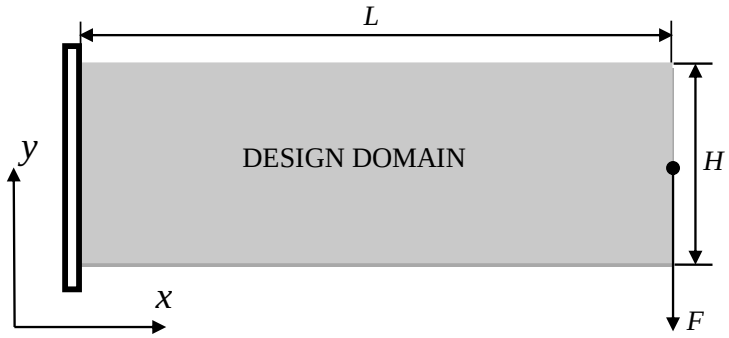


**Fig. 2** Design domain, boundary and loading

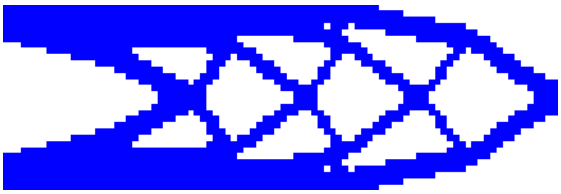

Deterministic design, $C = 2.4478$

**Fig. 3** Optimized result for non-piezoelectric structure

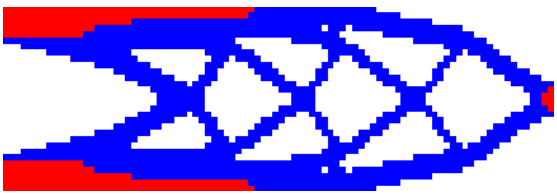

(a) Deterministic design, $C = 2.4121$

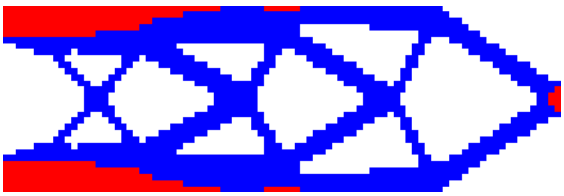

(b) Robust design, $\kappa = 1$, $C_{max} = 2.8016$

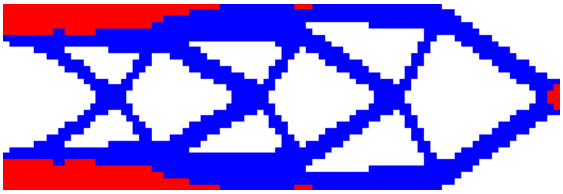

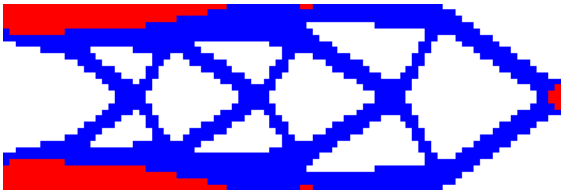

(c) Robust design, $\kappa = 3$, $C_{max} = 3.3791$ (d) Robust design, $\kappa = 5$, $C_{max} = 3.9669$

**Fig. 4** Optimized results for AS

**Table 1**

The maximal expectation and standard variance of the optimized results

| | | Maximal expectation | Relative errors | Maximal standard variance | Relative errors |
|---|---|---|---|---|---|
| Deterministic | MCM | 2.6008 | \ | 0.3202 | \ |
| | HUPAM | 2.5216 | 3.05% | 0.2975 | 7.09% |
| $\kappa = 1$ | MCM | 2.5806 | \ | 0.3193 | \ |
| | HUPAM | 2.5055 | 2.91% | 0.2961 | 7.26% |
| $\kappa = 3$ | MCM | 2.5768 | \ | 0.3144 | \ |
| | HUPAM | 2.4947 | 3.19% | 0.2948 | 6.23% |
| $\kappa = 5$ | MCM | 2.5757 | \ | 0.3142 | \ |
| | HUPAM | 2.4934 | 3.20% | 0.2947 | 6.21% |

*6.2 Example 2*

In this example, a beam shown in Fig. 5 is considered for optimization design with interval random uncertainties. The design domain is 80*mm* in length and 40*mm* in height which is divided into $80 \times 40$ quadrilateral elements. The lower left corner of the beam is clamped and the lower right corner is simply supported. Three external loads are applied on the lower bound of the model. The magnitudes of the loads are set to be 1*N*, 2*N* and 1*N* from the left side to the right side. For all robust optimization, the weight of the standard variance is set as $\kappa = 1$.

In order to explore the influence of the different interval random variables, the optimized results are shown in Fig .6. The variables based on the mechanical properties and the piezoelectric properties are divided into three kinds of uncertainties. Fig .6(a-c) is the robust designs corresponding to the mechanical and piezoelectric uncertainties, the mechanical uncertainties and the piezoelectric uncertainties. It can be observed that the final optimized structures are different. In Fig. 7(a), the objective function values of the non-piezoelectric structure with uncertainties are 1.5323 (for deterministic design) and 1.5310 (for robust design). Similarly, the objective function values of the AS with uncertainties are 1.5155 (for deterministic design) and 1.5126 (for robust design) in Fig .7(b). The values show that the robust topology optimization is better than the deterministic topology optimization when the uncertainties are considered. Compare Fig. 7(a) with Fig. 7(b), the objective function values for the AS are both smaller than those for the non-piezoelectric

structure, which means that the coupled structure provides better structural performance. Fig. 8 presents the convergent history of the robust optimization.

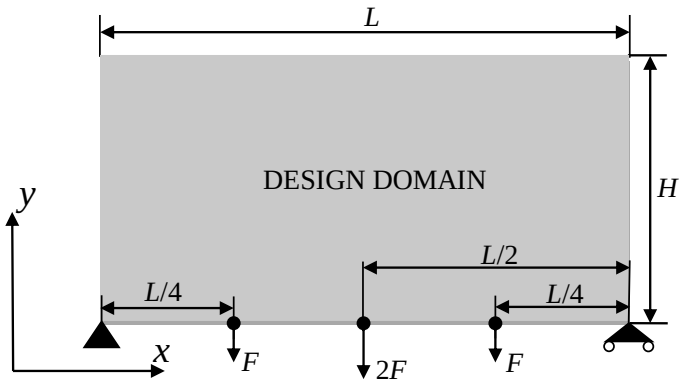


**Fig. 5** Design domain, boundary and loading

(a) Interval random variable ( $E$, $v$ *and* $e$ )

(b) Interval random variable ( $E$ *and* $v$ )

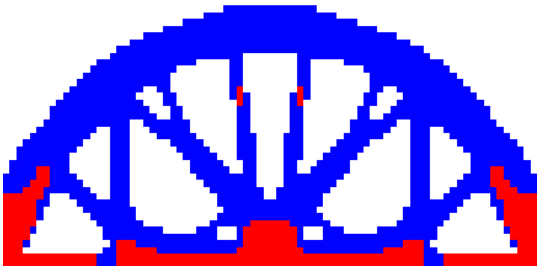

(c) Interval random variable ( $e$ )

**Fig. 6** Optimized results of robust design

(a1) Deterministic design, $C_{max}=1.5323$

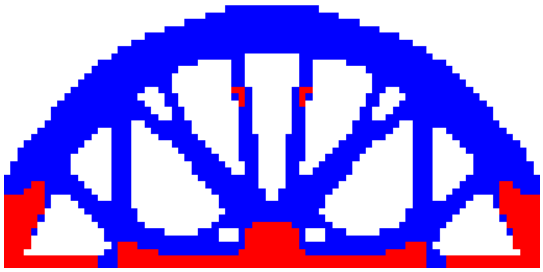

(b1) Deterministic design, $C_{max}=1.5155$

(a2) Robust design, $C_{max}=1.5310$

(b2) Robust design, $C_{max}=1.5126$

**Fig. 7** Optimized results for (a) non-piezoelectric structure (b) AS

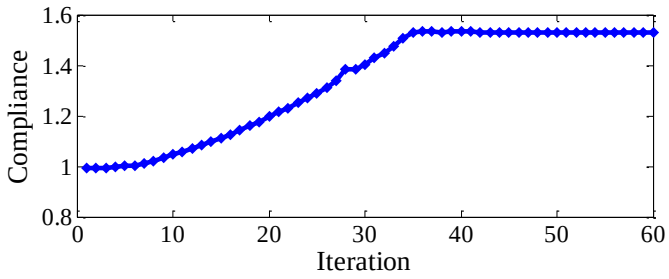


(a) Non-piezoelectric structure

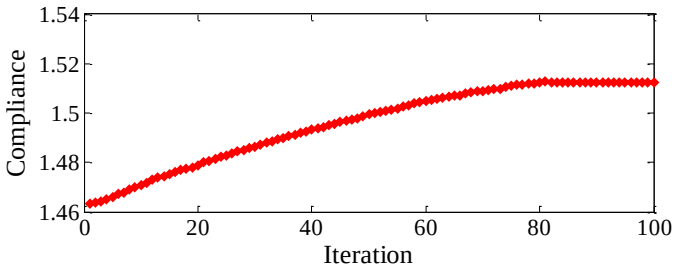


(b) Actuator-coupled structure

**Fig. 8** Convergent history of robust optimization

*6.3 Example 3*

Consider a structure with three boundary conditions, the constraints and loads are given in Fig. 9. The length of the design domain is 100*mm* and the height is 20*mm*. For all cases, the magnitude ( $F=10N$ ) and the position of the load are the same. The design domain is divided into $100\times 20$ quadrilateral elements. The weight of standard variance is set as $\kappa=1$.

Table 2 shows the deterministic designs and robust designs of three cases. It is obvious that the uncertain parameters have a significant effect on the structural shape and the actuators distribution. $E\left(C_d\right)_{max}$ and $SD\left(C_d\right)_{max}$ denote the maximal expectation and maximal standard variance of the robust objective function value. In all cases, $E\left(C_d\right)_{max}$ and $SD\left(C_d\right)_{max}$ of the robust optimized results are both smaller than those of the deterministic optimized results. From the above we can realize that the uncertainties

are worth being considered for structural design, and the structural performance of the robust designs is better than those of the deterministic designs.

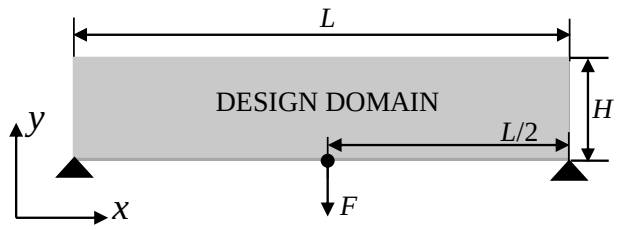


(a) Case 1

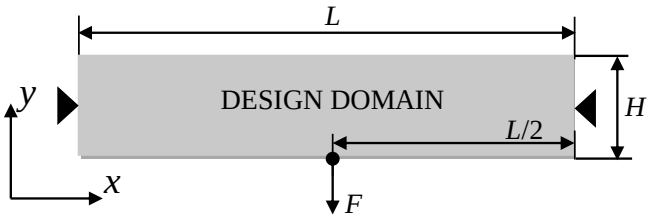


(b) Case 2

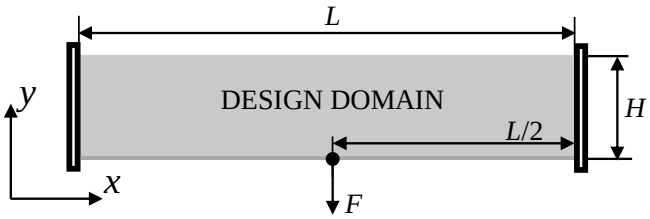


(c) Case 3

**Fig. 9** Design domain, boundary and loading for three boundary structures

**Table 2**

The optimized results and the robust objective function values

| | Deterministic designs | Robust designs |
|---|---|---|
| Case 1 |  |  |
| | $E(C_d)_{max}=50.0433,\ SD(C_d)_{max}=5.4129$ | $E(C_d)_{max}=49.4920,\ SD(C_d)_{max}=5.3512$ |
| Case 2 |  |  |
| | $E(C_d)_{max}=90.6234,\ SD(C_d)_{max}=10.6606$ | $E(C_d)_{max}=89.0029,\ SD(C_d)_{max}=10.5273$ |
| Case 3 |  |  |
| | $E(C_d)_{max}=37.9480,\ SD(C_d)_{max}=4.0952$ | $E(C_d)_{max}=37.9046,\ SD(C_d)_{max}=4.0863$ |

*6.4 Example 4*

Fig. 10 shows a square plate structure with the four edges that are set to be fixed. The design domain with the length $L = 40mm$ and the thickness $T = 1mm$, is discretized with $40 \times 40$ quadrilateral elements in plane and the single meshed quadrilateral element in the thickness direction. A concentrated load $F = 1N$ is applied at the center of the plane and the direction of the load is perpendicular to the plate. The weight of standard variance is set as $\kappa = 1$.

The optimized results with the deterministic parameters and uncertainties are given in Fig. 11. The robust design is different from the deterministic design, although they have similar topologies. In order to clearly show the structural robustness, the proposed method and MCM are adopted to calculate the maximal expectation and standard variance of deterministic design and robust design. In Table 3, the maximal expectation value and standard variance value of robust design are smaller than those of deterministic design which clearly illustrates the effectiveness of robust topology optimization. Besides, the robust objective function values of deterministic design for HUPAM and MCM are 1.6765 and 1.7089. The robust objective function values of robust design for HUPAM and MCM are 1.5811 and 1.6145, respectively. That means the proposed method can well simulate the uncertainties in the AS and achieves a better robust design.

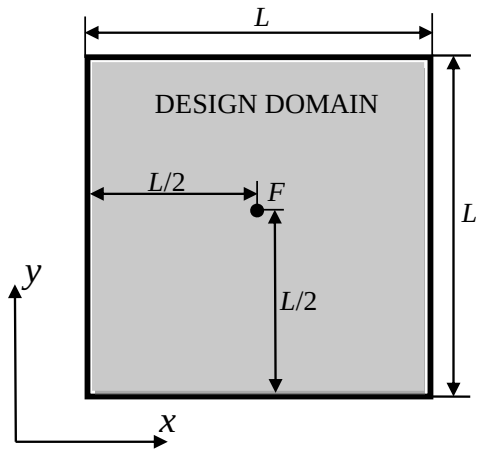


**Fig. 10** Design domain, boundary and loading

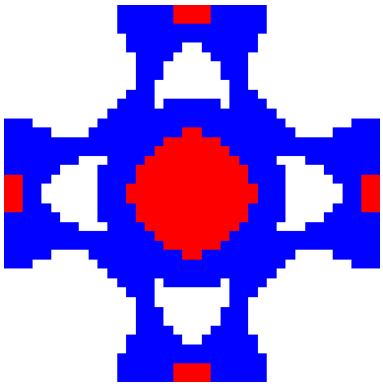

(a) Deterministic design

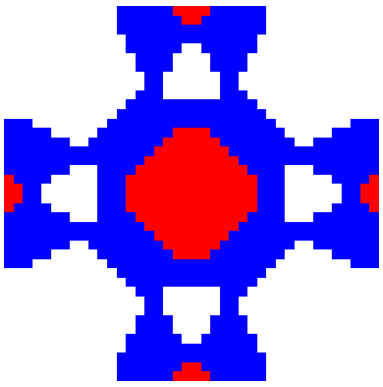

(b) Robust design

**Fig. 11** Optimized results for AS

**Table 3**

The maximal expectation and standard variance of the optimized results

| | | Maximal expectation | Maximal standard variance |
|---|---|---|---|
| Deterministic | MCM | 1.5336 | 0.1753 |
| | HUPAM | 1.5096 | 0.1669 |
| Robust | MCM | 1.4544 | 0.1601 |
| | HUPAM | 1.4286 | 0.1525 |

## 7. Conclusions

The piezoelectric actuator-coupled structures have obvious advantages in structural control. Nevertheless, further study is worthwhile in two aspects: the influence of the inevitable uncertainty in actual engineering and the topological design of coupling structures with imprecise uncertainty. To deal with these problems, this paper has developed a robust topology optimization method for the actuator-coupled structures subject to hybrid interval random variables. The hybrid uncertainty perturbation analysis method, which ensures the precision and reduces the computational expense, is used to estimate the expectation and standard variance of the objective function. The design results have shown that the actuator-coupled structures have better performance than the single structures, and the uncertainties have a significant effect on the optimized designs. The results calculated by the proposed hybrid uncertainty perturbation analysis method and the Monte Carlo method have demonstrated that the robust designs are better than the deterministic designs, and the proposed method is effective to deal with hybrid uncertainties.

## Acknowledgements

This work was supported by the National Key R&D Program of China（2016YFB0100903-2, the Foundation for Innovative Research Groups of the National Natural Science Foundation of China (Grant No. 51621004), the Opening Project of the Guangxi Key Laboratory of Automobile Components and Vehicle Technology of Guangxi University of Science and Technology (No. 2017GKLACVTKF01), and the opening project of the Hunan Provincial Key Laboratory of Vehicle Power and Transmission System (No. VPTS-2019-02, VPTS-2019-03 and VPTS-2019-06). In addition, the authors thanks to the reviewers for their constructive comments.

## Reference


1. Aridogan, U., Basdogan, I.: A review of active vibration and noise suppression of plate-like structures with piezoelectric transducers. Journal of Intelligent Material Systems and Structures **26**(12), 1455-1476 (2015). doi:10.1177/1045389X15585896
2. Wang, X., Zhou, J., Song, J., Liu, J., Xu, N., Wang, Z.L.: Piezoelectric field effect transistor and nanoforce sensor based on a single ZnO nanowire. Nano letters **6**(12), 2768-2772 (2006). doi:10.1021/nl061802g
3. Koconis, D.B., Kollar, L.P., Springer, G.S.: Shape Control of Composite Plates and Shells with Embedded Actuators. II. Desired Shape Specified. Journal of Composite Materials **28**(3), 262-285 (1994). doi:10.1177/002199839402800305
4. Kim, H.S., Kim, J.-H., Kim, J.: A review of piezoelectric energy harvesting based on vibration. International Journal of Precision Engineering and Manufacturing **12**(6), 1129-1141 (2011). doi:10.1007/s12541-011-0151-3
5. Zhang, X., Takezawa, A., Kang, Z.: Topology optimization of piezoelectric smart structures for minimum energy consumption under active control. Structural and Multidisciplinary Optimization **58**(1), 185-199 (2018). doi:10.1007/s00158-017-1886-y
6. Molter, A., Fonseca, J.S.O., Fernandez, L.d.S.: Simultaneous topology optimization of structure and piezoelectric actuators distribution. Applied Mathematical Modelling **40**(9), 5576-5588 (2016). doi:https://doi.org/10.1016/j.apm.2016.01.023
7. Li, C., Ding, Y., Gu, G., Zhu, L.: Damping Control of Piezo-Actuated Nanopositioning Stages With Recursive Delayed Position Feedback. IEEE/ASME Transactions on Mechatronics **22**(2), 855-864 (2017). doi:10.1109/TMECH.2016.2639584
8. Bendsoe, M.: Sigmund, Topology Optimization-Theory, Methods and Applications. In. Springer, (2003)
9. Bendsøe, M.P., Kikuchi, N.: Generating optimal topologies in structural design using a homogenization method. Computer Methods in Applied Mechanics and Engineering **71**(2), 197-224 (1988). doi:https://doi.org/10.1016/0045-7825(88)90086-2
10. Xie, Y.M., Steven, G.P.: A simple evolutionary procedure for structural optimization. Computers & Structures **49**(5), 885-896 (1993). doi:https://doi.org/10.1016/0045-7949(93)90035-C
11. Bendsøe, M.P., Sigmund, O.: Material interpolation schemes in topology optimization. Archive of Applied Mechanics **69**(9), 635-654 (1999). doi:10.1007/s004190050248
12. Wang, M.Y., Wang, X., Guo, D.: A level set method for structural topology optimization. Computer Methods in Applied Mechanics and Engineering **192**(1), 227-246 (2003). doi:https://doi.org/10.1016/S0045-7825(02)00559-5
13. He, Z.C., Zhang, G.Y., Deng, L., Li, E., Liu, G.R.: Topology Optimization Using Node-Based Smoothed Finite Element Method. International Journal of Applied Mechanics **07**(06), 1550085 (2015). doi:10.1142/S1758825115500854
14. Luo, Z., Tong, L., Wang, M.Y., Wang, S.: Shape and topology optimization of compliant mechanisms using a parameterization level set method. Journal of Computational Physics **227**(1), 680-705 (2007). doi:https://doi.org/10.1016/j.jcp.2007.08.011
15. Wu, J., Luo, Z., Li, H., Zhang, N.: Level-set topology optimization for mechanical metamaterials under hybrid uncertainties. Comput Method Appl M **319**, 414-441 (2017). doi:https://doi.org/10.1016/j.cma.2017.03.002
16. Nasser, H., Porn, S., Koutsawa, Y., Giunta, G., Belouettar, S.: Optimal design of a multilayered piezoelectric transducer based on a special unit cell homogenization method. Acta Mechanica **227**(7), 1837-1847 (2016). doi:10.1007/s00707-016-1581-x
17. Martin, K., Em ílio, C.N.S.: Topology optimization of smart structures: design of piezoelectric plate and shell actuators. Smart Materials and Structures **14**(2), 387 (2005).

18. Ronny, C.C., Emílio, C.N.S., Shinji, N.: Optimum placement of piezoelectric material in piezoactuator design. Smart Materials and Structures **16**(1), 207 (2007).
19. Zheng, B., Chang, C.-J., Gea, H.C.: Topology optimization of energy harvesting devices using piezoelectric materials. Structural and Multidisciplinary Optimization **38**(1), 17-23 (2009). doi:10.1007/s00158-008-0265-0
20. Kang, Z., Wang, R., Tong, L.: Combined optimization of bi-material structural layout and voltage distribution for in-plane piezoelectric actuation. Computer Methods in Applied Mechanics and Engineering **200**(13), 1467-1478 (2011). doi:https://doi.org/10.1016/j.cma.2011.01.005
21. Yiqiang, W., Zhen, L., Xiaopeng, Z., Zhan, K.: Topological design of compliant smart structures with embedded movable actuators. Smart Materials and Structures **23**(4), 045024 (2014).
22. Schuëller, G.I., Jensen, H.A.: Computational methods in optimization considering uncertainties – An overview. Computer Methods in Applied Mechanics and Engineering **198**(1), 2-13 (2008). doi:https://doi.org/10.1016/j.cma.2008.05.004
23. Wang, L., Xiong, C., Wang, X., Liu, G., Shi, Q.: Sequential optimization and fuzzy reliability analysis for multidisciplinary systems. Structural and Multidisciplinary Optimization **60**(3), 1079-1095 (2019). doi:10.1007/s00158-019-02258-y
24. Ghanem, R., Red-Horse, J.: Propagation of probabilistic uncertainty in complex physical systems using a stochastic finite element approach. Physica D: Nonlinear Phenomena **133**(1), 137-144 (1999). doi:https://doi.org/10.1016/S0167-2789(99)00102-5
25. Stefanou, G., Savvas, D., Papadrakakis, M.: Stochastic finite element analysis of composite structures based on mesoscale random fields of material properties. Computer Methods in Applied Mechanics and Engineering **326**, 319-337 (2017). doi:https://doi.org/10.1016/j.cma.2017.08.002
26. Massa, F., Tison, T., Lallemand, B.: A fuzzy procedure for the static design of imprecise structures. Computer Methods in Applied Mechanics and Engineering **195**(9), 925-941 (2006). doi:https://doi.org/10.1016/j.cma.2005.02.015
27. Wang, L., Wang, X., Xia, Y.: Hybrid reliability analysis of structures with multi-source uncertainties. Acta Mechanica **225**(2), 413-430 (2014). doi:10.1007/s00707-013-0969-0
28. Jiang, C., Zhang, Q.F., Han, X., Qian, Y.H.: A non-probabilistic structural reliability analysis method based on a multidimensional parallelepiped convex model. Acta Mechanica **225**(2), 383-395 (2014). doi:10.1007/s00707-013-0975-2
29. Jiang, C., Liu, N.Y., Ni, B.Y.: A Monte Carlo simulation method for non-random vibration analysis. Acta Mechanica **228**(7), 2631-2653 (2017). doi:10.1007/s00707-017-1842-3
30. Wang, L., Xia, H., Zhang, X., Lv, Z.: Non-probabilistic reliability-based topology optimization of continuum structures considering local stiffness and strength failure. Computer Methods in Applied Mechanics and Engineering **346**, 788-809 (2019). doi:https://doi.org/10.1016/j.cma.2018.09.021
31. Jiang, C., Zheng, J., Han, X.: Probability-interval hybrid uncertainty analysis for structures with both aleatory and epistemic uncertainties: a review. Structural and Multidisciplinary Optimization **57**(6), 2485-2502 (2018). doi:10.1007/s00158-017-1864-4
32. He, Z.C., Wu, Y., Li, E.: Topology optimization of structure for dynamic properties considering hybrid uncertain parameters. Structural and Multidisciplinary Optimization **57**(2), 625-638 (2018). doi:10.1007/s00158-017-1769-2
33. Wu, J., Luo, Z., Li, H., Zhang, N.: A new hybrid uncertainty optimization method for structures using orthogonal series expansion. Applied Mathematical Modelling **45**, 474-490 (2017).
34. Farrokh, M., Azar, A., Jandaghi, G., Ahmadi, E.: A novel robust fuzzy stochastic programming for closed loop supply chain network design under hybrid uncertainty. Fuzzy Sets and Systems **341**, 69-91 (2018). doi:https://doi.org/10.1016/j.fss.2017.03.019
35. Wu, D., Gao, W.: Hybrid uncertain static analysis with random and interval fields. Computer Methods in

Applied Mechanics and Engineering **315**, 222-246 (2017).
36. Xia, B., Yu, D.: An interval random perturbation method for structural-acoustic system with hybrid uncertain parameters. International Journal for Numerical Methods in Engineering **97**(3), 181-206 (2013). doi:10.1002/nme.4585
37. Xia, B., Yu, D., Han, X., Jiang, C.: Unified response probability distribution analysis of two hybrid uncertain acoustic fields. Computer Methods in Applied Mechanics & Engineering **276**(7), 20-34 (2014).
38. Kharmanda, G., Olhoff, N., Mohamed, A., Lemaire, M.: Reliability-based topology optimization. Structural & Multidisciplinary Optimization **26**(5), 295-307 (2004).
39. Kang, Z., Luo, Y.: Non-probabilistic reliability-based topology optimization of geometrically nonlinear structures using convex models. Computer Methods in Applied Mechanics and Engineering **198**(41), 3228-3238 (2009). doi:https://doi.org/10.1016/j.cma.2009.06.001
40. Zheng, J., Luo, Z., Jiang, C., Ni, B., Wu, J.: Non-probabilistic reliability-based topology optimization with multidimensional parallelepiped convex model. Structural and Multidisciplinary Optimization **57**(6), 2205-2221 (2018).
41. Wang, L., Liu, D., Yang, Y., Hu, J.: Novel methodology of Non-probabilistic Reliability-based Topology Optimization (NRBTO) for multi-material layout design via interval and convex mixed uncertainties. Computer Methods in Applied Mechanics and Engineering **346**, 550-573 (2019). doi:https://doi.org/10.1016/j.cma.2018.11.035
42. Jalalpour, M., Tootkaboni, M.: An efficient approach to reliability-based topology optimization for continua under material uncertainty. Structural and Multidisciplinary Optimization **53**(4), 759-772 (2016).
43. Wang, L., Liu, D., Yang, Y., Wang, X., Qiu, Z.: A novel method of non-probabilistic reliability-based topology optimization corresponding to continuum structures with unknown but bounded uncertainties. Computer Methods in Applied Mechanics and Engineering **326**, 573-595 (2017). doi:https://doi.org/10.1016/j.cma.2017.08.023
44. Dunning, P.D., Kim, H.A.: Robust Topology Optimization: Minimization of Expected and Variance of Compliance. AIAA Journal **51**(11), 2656-2664 (2013). doi:10.2514/1.J052183
45. Jansen, M., Lombaert, G., Diehl, M., Lazarov, B.S., Sigmund, O., Schevenels, M.: Robust topology optimization accounting for misplacement of material. Structural and Multidisciplinary Optimization **47**(3), 317-333 (2013). doi:10.1007/s00158-012-0835-z
46. Wu, J., Gao, J., Luo, Z., Brown, T.: Robust topology optimization for structures under interval uncertainty. Advances in Engineering Software **99**, 36-48 (2016). doi:https://doi.org/10.1016/j.advengsoft.2016.05.002
47. Chen, N., Yu, D., Xia, B., Ma, Z.: Topology optimization of structures with interval random parameters. Computer Methods in Applied Mechanics and Engineering **307**, 300-315 (2016).
48. Zheng, J., Luo, Z., Jiang, C., Gao, J.: Robust topology optimization for concurrent design of dynamic structures under hybrid uncertainties. Mechanical Systems and Signal Processing **120**, 540-559 (2019).
49. Haug, E., Choi, K., Komkov, V.: Design Sensitivity Analysis of Structural Systems. (1986)
50. Sigmund, O., Petersson, J.: Numerical instabilities in topology optimization: A survey on procedures dealing with checkerboards, mesh-dependencies and local minima. Structural optimization **16**(1), 68-75 (1998). doi:10.1007/BF01214002
51. Huang, X., Xie, Y.M.: Convergent and mesh-independent solutions for the bi-directional evolutionary structural optimization method. Finite Elements in Analysis and Design **43**(14), 1039-1049 (2007). doi:https://doi.org/10.1016/j.finel.2007.06.006